Acta Polytechnica CTU Proceedings **57**:81–89, 2026
https://doi.org/10.14311/APP.2026.57.0081

PEDESTRIAN MOTION ALONG CURVES: A COMPARATIVE STUDY OF DYADS AND INDIVIDUALS

Adrien Gregorj[a], Zeynep Yücel[b, c, *], Francesco Zanlungo[d, c], Takayuki Kanda[e, c]

[a] *Hitachi Ltd. R&D Group, Tokyo, Japan*
[b] *Ca' Foscari University of Venice, Department of Environmental Sciences, Informatics and Statistics, Venice, Italy*
[c] *Advanced Telecommunication Research Institute International, Kyoto, Japan*
[d] *University of Palermo, Department of Physics and Chemistry – Emilio Segrè, Palermo, Italy*
[e] *Kyoto University, Department of Social Informatics, Kyoto, Japan*
[*] corresponding author: zeynep.yucel@unive.it

Abstract. This study examines how individuals and dyads move along curved trajectories. By comparing velocities, path curvature, and their interplay across curved and straight segments, we identify distinct motion patterns. Specifically, dyads move more slowly than individuals on both straight and curved sections. Both individuals and dyads slow down as curvature increases, but individuals exhibit a slightly larger deceleration and more variability in curvature. However, these tendencies are modulated in certain environmental contexts, indicating context-dependent dynamics. Within dyads, the outer member covers longer distances with slightly lower curvature than the inner member, though the differences are modest. In curved segments, dyad members tend to balance their speeds, highlighting the need to account for intra-group roles in motion models and crowd-trajectory predictions.

Keywords: Social pedestrian groups, path curvature, velocity-path relationship.

1. Introduction

Crowds have a heterogeneous composition in terms of social relations [1, 2]. Most pedestrians walk alone (henceforth, "individuals"), while some pedestrians move together with others sharing social bonds and common goals (henceforth, "groups") [3]. In some cases, groups form a substantial portion of the crowd [4]. Among groups, dyads are most common, followed by triads; and larger groups (≥ 4), which often split into 2–3 people groups, highlighting the importance of small groups as building blocks for larger ones [5, 6].

This study focuses on dyads, comparing their path choices to those of individuals. Our main question is: do dyads select routes differently from individuals? More precisely, we consider a relatively simple environment where movement predominantly consists of straight segments connected by junctions. At these junctions, pedestrians must negotiate curves, and we aim to investigate whether dyads tend to adopt particular trajectory shapes or exhibit different velocity profiles in such scenarios. Additionally, we seek to understand the underlying reasons for any observed differences. To achieve this, we analyze whether the curvatures of the paths chosen by dyads differ from those of individuals, whether dyads display distinct velocity patterns on curved sections, and how curvature relates to velocity.

2. Background and related work

A common framework for pedestrian dynamics describes three levels: strategic (destination choice), tactical (route selection to reach that goal), and operational (interactions with others and the environment along the route) [7]. In this study, we aim to simplify the scenario by excluding from the definition of referecence trajectories (see Section 4) interactions with other moving obstacles to focus on understanding how the topology of the environment influences pedestrians' path choices. This may be positioned somewhat between the tactical and operational levels and is not treated often in previous literature.

From a purely mathematical perspective, the choice of velocity along a path does not necessarily depend on or correlate with the topology of that path. However, various observations on movement of human body parts, or biological motion at large, indicate a dependence [8, 9]. Specifically, an inverse relationship between the speed and curvature is reported for various hand, eye, limb movements [10].

As for pedestrian walking motion, studying collision avoidance and path planning along straight paths under diluted conditions is common [11]. Along straight paths, people tend to move on nearly straight trajectories. However, obstacles, infrastructure, and crowd dynamics frequently induce curved trajectories [12–14]. Under such low-density conditions, straight-path models can capture average motion reasonably well [15]. Nevertheless, for curved paths, the validity of straight-

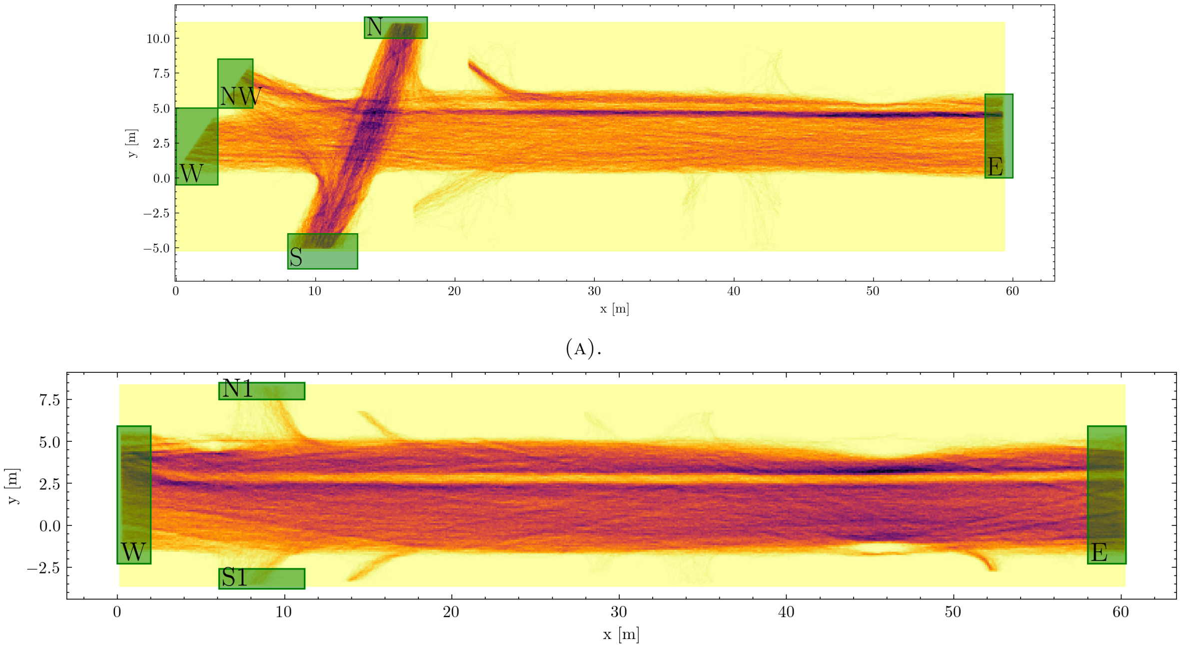

(A).

(B).

Figure 1. The normalized cumulative density map for the DIAMOR dataset. The recordings were taken in two different parts DIAMOR underground street network shown in (A) and (B). The recording area is divided into a grid of 10 cm × 10 cm cells. Then, the number of pedestrians present in each cell at any point in time is tallied. These counts are subsequently normalized by the maximum count observed across the entire grid. In the resulting maps, darker regions denote areas with higher pedestrian density. Sources/sinks are overlayed with green rectangles.

path models depends on the curvature radius. Although several studies have explored the relationship between curvature and path geometry, there is no experimental consensus on how curvature affects pedestrians' dynamics [16, 17]. Moreover, the literature lacks a clear investigation of such relationship in case of pedestrian group motion, a gap this study seeks to fill.

3. Data set and preprocessing

This work uses a publicly available data set [18] containing pedestrian trajectories together with group annotations[1]. The data set was first introduced in [19] and since then it has been extensively used in research on pedestrian dynamics [20–22].

The trajectories were collected in the DIAMOR underground street network, a facility that is exclusively used by pedestrians, connecting several stations, shopping centers and ground level. The experiment zone constitutes part of the Umeda (Central Osaka) station system, which is the fourth busiest station network in the world with an impressive passenger rate of over 2 million per day [23–26]. Nevertheless, in the specific area and time in which data were collected, crowd density was in the low-medium range (0.02–0.03 ped m^{-2}) [19], allowing for good tracking and fluid pedestrian motion.

[1] Experimentation has been reviewed and approved by ATR ethics board (Document number 10-502-1).

Raw data includes two streams, namely range readings and video. In particular, two distinct corridors were equipped with a system of laser range sensors. The raw range data were processed to extract trajectories [27] (see Figure 1). In addition, a network of video cameras recorded footage, which human coders used to identify pedestrians walking alone (individuals) and those who appeared to be part of a social group (dyads, triads, etc.).

We identified nine rectangular areas that define entry/exit points of the environment, which we call “sources” or “sinks” (see Figure 1). All trajectories of individuals and dyads traversing between any source-sink pair were extracted. It is important to note that any of the zones highlighted by green rectangles in Figure 1 can function as both a source and a sink, as pedestrians may enter or leave the environment through these areas. Conversely, a designated source-sink pair, e.g. NW-S in Figure 2a, explicitly delineates the entry and exit zones.

Taking a closer look, we noticed that some trajectories exhibit unusual behaviors, such as making unexpectedly sharp or abrupt turns, displaying confused patterns like changing direction midway and reversing course, or experiencing tracking errors, such as swapping the identities of pedestrians exiting and entering the environment. In order to exclude such cases, concerning each source-sink pair s_1, s_2, we built an occupancy grid similar to the one in Figure 1. Specifically, we divided the environment into 0.5 m × 0.5 m grid cells and projected all trajectories $\{\tilde{T}_i\}$ traversing between s_1, s_2 onto it. After computing a 2D histogram in this manner, we counted for each trajectory $\tilde{T}_i$ the number of cells with a single observation. If the number of such observations exceed 10 % of the trajectory points, we discarded that trajectory.

At the end of this operation, we obtained a total of 1 250 dyads[2] and 9 247 individuals to be used in subsequent analysis.

4. Method

We compute a reference trajectory between each source-sink pair [28][3], which represents the average path taken by all pedestrians tracing between that source-sink pair. To obtain these trajectories, we first normalize each individual trajectory to a fixed number of data points, as described in Section 4.1, and then take the average of the normalized trajectories as explained in Section 4.2.

4.1. Normalized trajectories

To normalize the trajectories traversing between a source-sink pair s_1, s_2, we first choose an appropriate number of data points, $N^{bins}_{s_1,s_2}$, that provides sufficient resolution while reducing stochastic fluctuations. We then apply binning along the arc length of the trajectories.

Consider a source-sink pair s_1, s_2. We compute the Manhattan distance[4] d_{s_1,s_2} taken from the center of the rectangular areas representing the source and the sink. We then divide d_{s_1,s_2} into segments (bins) of length $D^{bin} = 0.5\,\mathrm{m}$. The number of data points, $N^{bins}_{s_1,s_2}$, to be used in normalizing the trajectories traversing between s_1 and s_2[5] is then

$$N^{bins}_{s_1,s_2} = \left\lfloor \frac{d_{s_1,s_2}}{D^{bin}} \right\rfloor . \tag{1}$$

Let all trajectories relating to e.g. individuals, traversing from s_1 to s_2 be $\{T_i\}$, where $T_i = \{\mathbf{p}_i(t_{i,j})\}$. Here, $\mathbf{p}_i$ is the position of pedestrian i at time $t_{i,j}$, which is the jth sample of T_i. Note that $j \in [1, K_i]$ as K_i denotes T_i's total number of samples.

To obtain the spatial binning of T_i, we first calculate its arc length. Let $\ell_i(k)$ denote the arc length of T_i from the first to the kth sample,

$$\ell_i(k) = \sum_{j=1}^{k-1} \left\| \mathbf{p}_i(t_{i,(j+1)}) - \mathbf{p}_i(t_{i,j}) \right\| . \tag{2}$$

We then divide $\ell_i(K_i)$ into $N^{bins}_{s_1,s_2}$ bins and assign each $\mathbf{p}_i$ to the corresponding bin b_m,

$$b_m = \left\{ j \mid (m-1) \cdot D^{bin} < \ell_i(j) \leq m \cdot D^{bin} \right\} ,$$

with $m \in [1, N^{bins}_{s_1,s_2}]$. Averaging the positions and times in each bin, we obtain the normalized trajectory $\tilde{T}_i = \left\{ \tilde{\mathbf{p}}_i(\tilde{t}_{i,j}) \right\}$ concerning the raw trajectory T_i

$$\begin{aligned} \tilde{t}_{i,j} &= \langle t_{i,k} \rangle_{k \in b_j} \\ \tilde{\mathbf{p}}_i(\tilde{t}_{i,j}) &= \langle \mathbf{p}_i(t_{i,k}) \rangle_{k \in b_j} , \end{aligned} \tag{3}$$

where the operator $\langle \cdot \rangle$ denotes average.

4.2. Reference trajectories

The normalized trajectories $\left\{ \tilde{T}_i \right\}$ relating to s_1, s_2 are averaged to obtain the reference trajectory. $\mathcal{T} = \{\boldsymbol{\pi}(\tau_j)\}$, where

$$\begin{aligned} \tau_j &= \sum_i \tilde{t}_{i,j} / N, \\ \boldsymbol{\pi}(\tau_j) &= \sum_i \tilde{\mathbf{p}}_i(\tilde{t}_{i,j}) / N, \end{aligned} \tag{4}$$

N representing the number of trajectories traversing from source s_1 to sink s_2. This process generates a reference trajectory for each source-sink pair s_1, s_2 with $N^{bins}_{s_1,s_2}$ points of average position $\boldsymbol{\pi}$ and time τ_j.

We apply this procedure to obtain the reference trajectory between all possible source-sink pairs s_1, s_2 and for dyads and individuals, separately. The resulting reference trajectories are denoted as $\mathcal{T}^{dyad}_{s_1,s_2}$ and $\mathcal{T}^{ind}_{s_1,s_2}$.

4.3. Curvature

Considering a generic 2D trajectory $\mathbf{r}(t) = (x(t), y(t))$, its velocity and acceleration are[6]

$$\begin{aligned} \mathbf{v}(t) &= (v_x(t), v_y(t)) = (\dot{x}(t), \dot{y}(t)) , \\ \mathbf{a}(t) &= (a_x(t), a_y(t)) = (\ddot{x}(t), \ddot{y}(t)) , \end{aligned} \tag{5}$$

Then the curvature κ of $\mathbf{r}(t)$ can be computed as [30]

$$\kappa(\mathbf{r}(t)) = \frac{|v_x(t)a_y(t) - v_y(t)a_x(t)|}{\|\mathbf{v}(t)\|^3} . \tag{6}$$

This corresponds to the inverse of the radius of a circular path approximating the trajectory in the point $\mathbf{r}(t)$. As it is clear from this geometrical meaning, the value of the curvature does not depend on the parametrization t, i.e. on the velocity the curve is traversed with.

Note that in Section 5.1.2, curvature will be displayed on a logarithmic scale within the graphs, since this highlights the changes in κ better. Readers should also keep in mind that on such log scale large negative values of curvature indicate trajectories that are nearly straight, whereas values closer to zero correspond to trajectories with greater curvature.

[2]We have 2 500 trajectories associated with dyads, since each dyad involves two members.

[3]This implies that the reference trajectory relating source s_1 and sink s_2 is different than the reference trajectory relating source s_2 and sink s_1.

[4]Here, Manhattan distance provides a first approximation to the walking distance considering a turn of $\pi/2$.

[5]Note that the value of $N^{bins}_{s_1,s_2}$ is the same for source-sink pairs of s_1, s_2 and s_2, s_1.

[6]Velocity and acceleration are computed by taking consecutive differences on the position and velocity arrays, respectively, and scaling with the sampling time window, which is 0.33 sec on average. In addition, to reduce noise in the trajectories, we initial applied a Savitzky-Golay filter to these positions [29] with a window of 0.25 s and a polynomial order of 2.

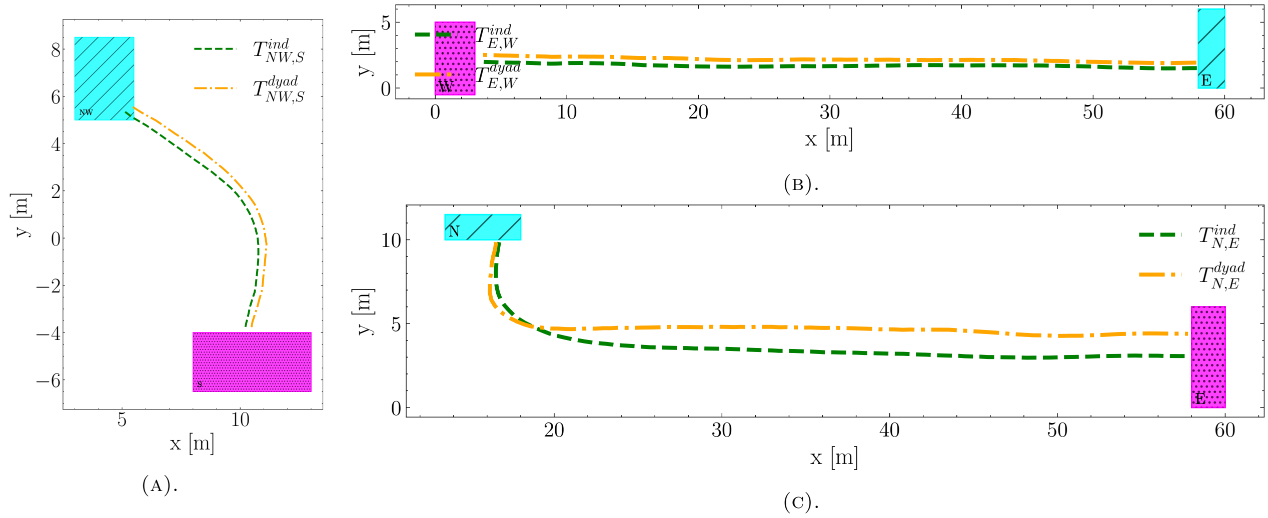

Figure 2. Examples of reference trajectories. Green dashed lines correspond to individuals and orange dash-dotted lines correspond to dyads. Cyan striped areas show entry zones and magenta dotted areas show exit zones.

4.4. Identifying inner and outer members

We call the dyad member who is walking closer to the corner "inner" and the other one "outer". Suppose that a dyad d with members a and b walks over a curved path along trajectories $T_{a,b} = \{\mathbf{p}_{a,b}(t_d)\}$ where positions $\mathbf{p}_{a,b}$ are sampled at simultaneous times t_d. Then, the velocities $\mathbf{v}_{a,b}(t_d)$ can simply be computed as the first derivatives of positions $\mathbf{p}_{a,b}$[7].

To determine which member of the dyad is inner and which is outer, we first compute the dyad's geometrical center of mass trajectory $T_d = \{\mathbf{p}_d(t_d)\}$.

Next, we transform the trajectories of a and b into a reference frame that moves together with the dyad d. Specifically, at each time instant t_d, the positions $\mathbf{p}_{a,b}$ are translated so that the dyad's center of mass $\mathbf{p}_d(t_d)$ shifts to the origin. In addition, they are rotated such that the group's overall velocity is aligned along the positive x-axis.

Let's denote the distance from a to b along the y-axis of this new reference frame as $\delta_y(a,b)$. This value represents the distance between the dyad members perpendicular to their direction of motion. If the dyad moves entirely side-by-side, $\delta_y(a,b)$ is equal to their interpersonal distance, whereas it boils down to zero, if they move exactly in a single file [5].

If $\delta_y(a,b) > 0$, then member a is on the left; otherwise, member b is on the left. Using this information along with the trajectory's source and sink positions, we can determine which of the left and right members corresponds to the inner or outer within the dyad based on the direction of the turn.

5. Results and discussion

5.1. Qualitative observations

In this section, we choose three sample source-sink pairs, present their reference trajectories and illustrate how velocity and curvature change along those.

5.1.1. Reference trajectories

In Figure 2, reference trajectories are depicted for three sample source-sink pairs with green dashed lines for individuals and orange dash-dotted lines for dyads[8]. Sources and sinks are indicated by cyan striped rectangles and magenta dotted rectangles, respectively.

In Figure 2a, we observe that dyads tend to follow a larger softer curve compared to individuals. Additionally, dyads generally remain on the left side of the individuals. Since in this environment pedestrian traffic predominantly flows on the left, this positioning indicates that individuals walk in general closer to the centerline of the corridor. This was to be expected since, as we will see later in Section 5.1.2, individuals are faster than dyads, agreeing with the findings of [31, 32], and faster pedestrians are expected to walk closer to the centerline of the street [31].

Figure 2b presents similar information for a path without any distinct curves. In this situation individuals and dyads follow an almost identical path, although, contrasting with Figure 2a, the position of the dyad is slightly closer to the centerline of the environment than the one of the individuals. Although it may seem surprising, based on the results of [31], that the slower dyads are, for this particular source-sink pair, closer to the middle of the corridor, it should be taken in account that dyads occupy a larger space than individuals, and this effect may be prevalent depending on the path and environment.

For the reference trajectories corresponding to the source-sink pair shown in Figure 2c we see that the dyads make a sharper curve than individuals in contrast with the case shown in Figure 2a. We notice also that in this case the faster individuals [32, 33] are

[7] A Savitzky-Golay filter is applied on the gradients for smoothing.

[8] We have chosen the source-sink pairs in Figure 2 such that there is one example for each of a straight path, a right-angle path and a not-right-angle path (subfigures b, c, a, respectively).

the ones walking closer to the centerline, in agreement with [31].

These figures indicate that dyad paths can feature softer or sharper curves, and their positioning along lanes (and potentially their velocities) may vary with changing environments, or even just by considering different source-sink pairs. Consequently, the relationship between curvature and velocity is likely not straightforward and influenced by a variety of intricate factors. In the following sections, we will explore this relationship in more detail.

By comparing the (not shown) reference trajectories of the inner and outer members, we notice that in general the outer member follows a slightly longer path and a thus a softly curved path than the inner, owing to their configuration.

5.1.2. Velocity and curvature

In Figure 3, we depict velocity v and log-curvature $\log(\kappa)$ profiles[9] concerning reference trajectories between the same sample source-sink pairs shown in Figure 2.

We notice in Figure 3a that the velocities of individuals and dyads are quite similar, in contrast with most findings in previous studies [33] and also in other source-sink pair in this environment. Nevertheless, if our observation range were expanded to include a broader span (i.e. covering past and future segments of the path, including straight sections), we would likely detect differences in velocities. As for log-curvature, we can see that there is a difference at the beginning and the end of the course. Namely, as λ denotes the normalized arc length, such difference can be seen for $\lambda < 0.2$ and $\lambda > 0.8$, but not in between.

In Figure 3b, which relates a path without any clear curves, we observe that dyads tend to move more slowly than individuals. We would like to highlight two interesting points here. First, as discussed in Section 5.1.1, for this source-sink pair, dyads are generally (slightly) positioned to the right of individuals. While it is expected that velocities are higher toward the centerline of the street compared to areas closer to the border, a closer examination of the velocity data reveals that, despite walking nearer to the center than individuals, dyads still move with a slower velocity. Another interesting observation is that the dyads slow down even further for $0.1 < \lambda < 0.4$, where the street intersects with another street (see also Figure 1). This behavior is likely due to collision avoidance, which requires a more complex planning for dyads compared to individuals. We also notice that the bottom part of Figure 3b does not present any considerable variation in curvature suggesting indeed that the change in velocity of dyads is related to collision avoidance and not curvature effects.

[9]Note that in the graphs we display $\log(\kappa)$ and in the tables we report κ. This choice is motivated by the fact that taking the logarithm of κ in the graphs magnifies the variability in the curved regions (see Figure 2).

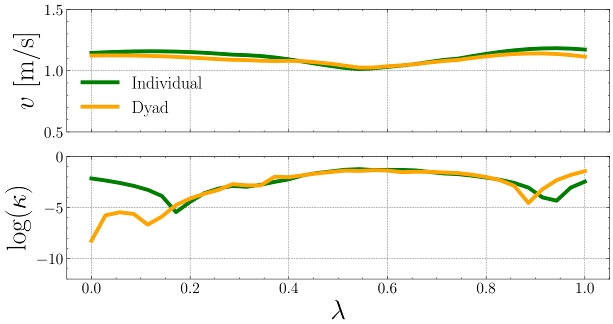

(a).

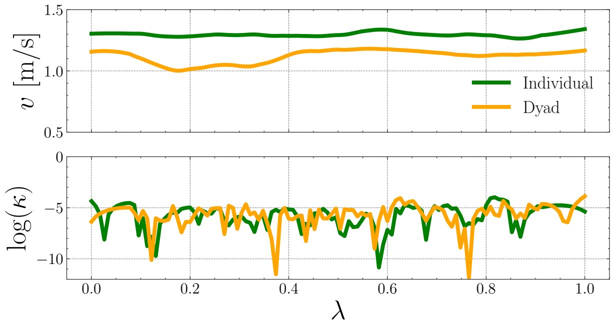

(b).

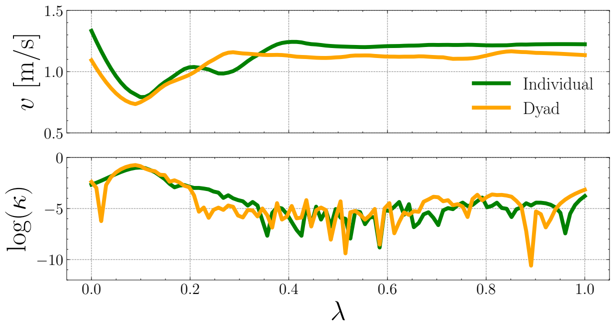

(c).

Figure 3. Sample velocity v (top) and log-curvature ($\log(\kappa)$, bottom) profiles with respect to normalized arc length λ. Parts (a-c) relate the same reference trajectories shown in Figure 2, respectively. Before taking the logarithm κ was measured in $[1\,\mathrm{m}^{-1}]$.

Finally, in Figure 3c on the top panel, we can see that both individuals and dyads are slower while curving, with dyads reaching a lower velocity. Interestingly, dyads are briefly faster than individuals when changing from the curved section to the straight section of the course, i.e. $0.25 < \lambda < 0.35$. Along the straight part, i.e. $\lambda > 0.4$, dyads move consistently with a lower velocity than individuals. At the bottom panel, the $\log(\kappa)$ values are seen to be higher and similar to one another at the curved section of the course, while they are quite low in the straight section, i.e. $\log(\kappa) \approx -5$ for $\lambda > 0.4$.

5.2. Quantitative assessment

In this section, our goal is to achieve a more comprehensive and quantitative assessment of velocity and log-curvature profiles. To accomplish this, we move

	v			κ		
	Mean	**Std dev.**	**Std err.**	**Mean**	**Std dev.**	**Std err.**
Individual	1.23	8.58×10^{-2}	2.56×10^{-3}	4.30×10^{-2}	7.66×10^{-2}	2.28×10^{-3}
Dyad	1.11	9.51×10^{-2}	3.60×10^{-3}	3.30×10^{-2}	6.82×10^{-2}	2.59×10^{-3}
Inner	1.09	1.07×10^{-1}	4.07×10^{-3}	3.70×10^{-2}	7.73×10^{-2}	2.93×10^{-3}
Outer	1.11	9.63×10^{-2}	3.65×10^{-3}	3.47×10^{-2}	6.20×10^{-2}	2.35×10^{-3}

TABLE 1. Descriptive statistics for v and κ.

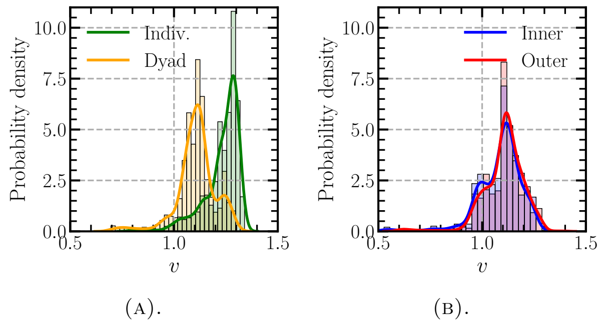

FIGURE 4. Histogram of v for (a) individuals and dyads and (b) inner and outer members of dyads. Solid lines depict kernel density estimations.

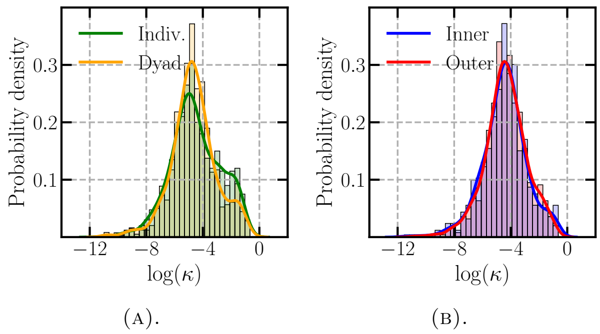

FIGURE 5. Histogram of $\log(\kappa)$ for (a) individuals and dyads and (b) inner and outer members of dyads. Solid lines depict kernel density estimations.

beyond the analysis of just the three sample source-sink pairs illustrated in Figure 2 and instead consider all possible source-sink pairs. We frame the discussion around statistics, distributions and bivariate plots.

5.2.1. Descriptive statistics and distributions

Table 1 shows descriptive statistics for velocity v and curvature κ for individuals, dyads and their inner and outer members.

Concerning velocity v, we can see that individuals are on average faster than dyads, while inner and outer members have very similar velocities with the inner one being slightly slower.

Concerning curvature κ, it is evident that, on average, individuals tend to have higher and more variable curvature values compared to dyads. This suggests that, overall, dyads tend to make softer curves.

When comparing the inner and outer members of dyads, we observe that the outer members generally display lower curvature values, as to be expected since the need to cover slightly longer walking distances. However, this observation is likely not conclusive, as the difference between inner and outer members is smaller than the standard errors of their curvature measurements.

To provide a more comprehensive overview, Figures 4 and 5 display the distributions of velocity v and the logarithm of curvature, $\log(\kappa)$, respectively. In Figure 4a, we observe that dyads tend to be slower than individuals. Figure 4b indicates that the inner and outer members of dyads overall have quite similar velocities, with the inner one slightly slower.

In Figure 5a, it becomes apparent that individuals more frequently walk at higher curvatures than dyads, with the most notable difference appearing around $-6 < \log(\kappa) < -1$. Conversely, the inner and outer members exhibit relatively similar curvature distributions, as shown in Figure 5b.

5.2.2. Velocity-curvature relation

Figure 6 shows the velocity v as a function of the logarithm of curvature $\log(\kappa)$[10]. From this plot, we observe that individuals are faster than dyads for any curvature value. Furthermore, the velocities of both individuals and dyads are insensitive to curvature for $\log(\kappa) < -5$. Beyond this, roughly around $\log(\kappa) \approx -4$, both individuals and dyads begin to feel the curvature and decelerate.

As $\log(\kappa)$ increases from -5 to -1, the velocity of individuals decreases from $1.27\,\mathrm{m\,s^{-1}}$ to $0.97\,\mathrm{m\,s^{-1}}$, while the velocity of dyads decreases from $1.12\,\mathrm{m\,s^{-1}}$ to $0.86\,\mathrm{m\,s^{-1}}$s. Consequently, the decrease in velocity due to curvature is slightly stronger for individuals than for dyads (about $0.30\,\mathrm{m\,s^{-1}}$ vs. $0.26\,\mathrm{m\,s^{-1}}$).

Furthermore, while individuals consistently slow down with increasing curvature for $\log(\kappa) > -5$, the decrease in velocity for dyads seems to be mostly limited to the $-4 < \log(\kappa) < -3$ and $\log(\kappa) > -1.5$ ranges. Thus, the velocity-curvature relationship for dyads appears to be less straightforward (i.e. more heterogeneous) than that for individuals.

To better understand this nontrivial aspect of dyad motion and, more generally, in-group dynamics, Figure 7 plots the velocity-curvature relation for the inner

[10] Note that, in computing the values reported in Figure 6, we used uniform bin sizes. This approach allowed us to pool between 275 and 23 values for the individuals and from 244 to 13 values for the dyads within each bin.

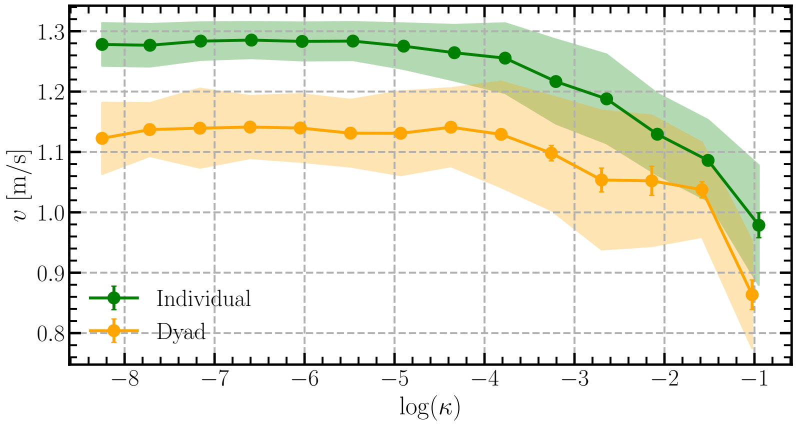

FIGURE 6. Velocity v against logarithm of curvature $\log(\kappa)$ for individuals and dyads for all source-sink pairs. Before taking the logarithm κ was measured in $[1\,\mathrm{m}^{-1}]$. Filled circles denote mean values and shaded regions indicate standard error.

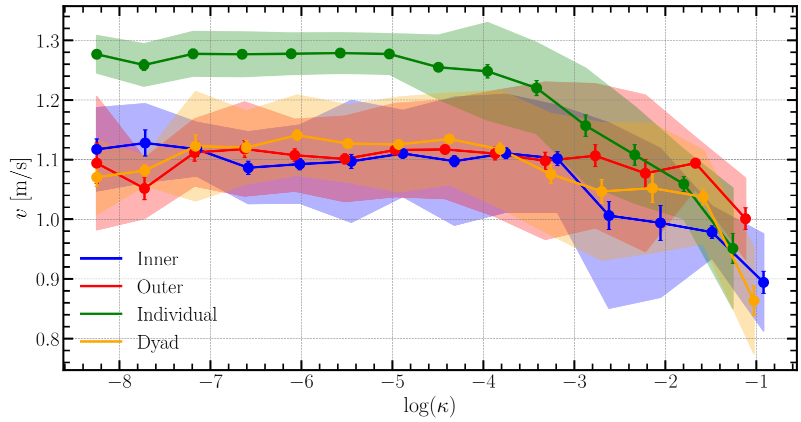

FIGURE 7. Velocity v against logarithm of curvature $\log(\kappa)$ for individuals, dyads and their inner and outer members (only those source-sink pairs that require a clear turn). Before taking the logarithm κ was measured in $[1\,\mathrm{m}^{-1}]$. Filled circles denote mean values and shaded regions indicate standard error.

and outer members of dyads[11]. Note that while Figure 6 includes all possible source-sink pairs, Figure 7 shows only the pairs that exhibit a clear turn, since the inner and outer roles are not defined otherwise. For reference, we also display the velocity-curvature relation for individuals and dyads for the same paths in Figure 7.

From this figure, we can see that the inner member decelerates sharply around $\log(\kappa) = -3$, while the outer member maintains its velocity as curvature increases. This pronounced drop occurs when the inner's velocity approaches that of the individuals at the corresponding curvature. Interestingly, for $\log(\kappa) > -2$, the inner member can even move faster than the individual. Overall, the inner member decelerates about twice as much as the outer (roughly $0.2\,\mathrm{m\,s}^{-1}$ versus $0.1\,\mathrm{m\,s}^{-1}$, respectively). These observations suggest that there is probably a need for different velocities for inner and outer members, since the outer has to walk more than the inner.

6. Limitations and future work

We have seen that certain source-sink pairs are traversed less often than others, possibly due to the fact that the end points of those paths did not lead to busy areas. Such reference trajectories are inherently more prone to noisy behavior and yet they are represented with a reference trajectory in the same way as the other more busy source-sink pairs. We believe that this is an inherent drawback of ecological data. In addition, the analyzed data is collected at a single location (country) and thus cultural variability cannot be addressed. Since pedestrian behavior as well as social norms and conventions may depend on culture, it is necessary to confirm the observations on data collected in other countries.

As future work, we plan to deepen our analyses as follows. Firstly, direction of turns may potentially influence curving dynamics. In left-hand traffic, a clock-

[11]Note that, in computing the values reported in Figure 7, we performed a binning to 14 bins (i.e. same number of bins as in Figure 6) ensuring also that each bin contained approximately the same number of values. This approach allowed us to pool 42 to 43 values for the dyads, and their inner and outer members, and 36 to 37 values for the individuals. The reader may notice that although the bin centers are not exactly at same locations as Figure 6, they are not much different.

wise turn requires crossing one flow and merging into another, whereas a counterclockwise turn mainly involves merging into another flow without any crossing. Therefore, we plan to partition source–sink pairs into two sets, i.e. those requiring clockwise turns and those requiring counterclockwise turns. As a benchmark, it would be better also to analyze some trajectories collected in a path with a corner and not in an intersection (i.e. with only turning and without merging or crossing any flows)[12]. Another aspect worth investigating is the alignment of the two members of dyads. On straight sections of course, the dyad is expected to be roughly abreast [5, 34], but the relative positioning of the inner and outer members over curved sections of the course deserves closer scrutiny.

7. Conclusions

This study examines the motion of individuals and dyads by comparing reference trajectories, velocities, and curvature, and by quantifying how they interact across curved and straight sections of the path.

Our qualitative and quantitative analyses reveal distinct motion patterns between individuals and dyads across varied path geometries. Reference trajectories show that dyads may traverse softer curves and position themselves on the left of individuals, consistent with leftward pedestrian flow and slower speeds in many zones, though exceptions occur depending on the environment. This indicates that dyad dynamics are not fixed and depend on local route geometry and context.

Velocity and curvature analyses demonstrate that, on average, individuals move faster than dyads. Descriptive statistics indicate higher mean velocity and greater variability in curvature for individuals, whereas dyads move softer and their curvature variability is smaller. In dyads, the outer member tends to cover slightly longer paths and shows marginally lower curvature than the inner member, though the magnitude of this difference is small relative to measurement variability.

The velocity-curvature relationship is interesting. Both individuals and dyads slow down as curvature increases, but the deceleration is slightly stronger for individuals. Interestingly, during straight segments, dyads generally maintain lower speeds than individuals consistently and irrespective to the position of the member, while in curved segments, the two members seek for a balance in their velocities. The inner displays a pronounced deceleration around moderate curvature, while the outer maintains velocity more robustly, suggesting the necessity to accommodate different velocity profiles when planning group motion.

Overall, the findings highlight that dyad dynamics, particularly intra-group roles (inner vs outer), modulate speed and turning behavior in ways that are not simply extrapolated from individual motion. These insights are crucial for refining pedestrian motion models and crowd-trajectory predictions in realistic environments with varying curvature.

[12] Of course, one can also go further by considering corners or intersection with different angles etc.

Acknowledgements

This work was in part supported by JST Moonshot R and D under Grant Number JPMJMS2011, Japan, and in part supported by JSPS KAKENHI Grant No. 24H00722, Japan. This study was partially supported by the Japan Society for the Promotion of Science (JSPS) under Grant-in-Aid for JSPS Fellows with Grant Number 22J20686.

References

[1] M. Schultz, L. Rößger, H. Fricke, B. Schlag. Group dynamic behavior and psychometric profiles as substantial driver for pedestrian dynamics. In *Pedestrian and Evacuation Dynamics 2012*, pp. 1097–1111. Springer, 2014. https://doi.org/10.1007/978-3-319-02447-9_90

[2] J. Adrian, M. Amos, C. Appert-Rolland, et al. Glossary for research on human crowd dynamics – 2nd edition. *Collective Dynamics* **10**:1–32, 2025. https://doi.org/10.17815/CD.2025.189

[3] C. McPhail, R. T. Wohlstein. Using film to analyze pedestrian behavior. *Sociological Methods & Research* **10**(3):347, 1982. https://doi.org/10.1177/0049124182010003007

[4] M. Moussaïd, N. Perozo, S. Garnier, et al. The walking behaviour of pedestrian social groups and its impact on crowd dynamics. *PLoS ONE* **5**(4):e10047, 2010. https://doi.org/10.1371/journal.pone.0010047

[5] F. Zanlungo, T. Kanda. Do walking pedestrians stabily interact inside a large group? Analysis of group and subgroup spatial structure. In *COGSCI13 (2013 Cognitive Science Society Conference)*, pp. 3847–3852. 2013.

[6] M. Costa. Interpersonal distances in group walking. *Journal of Nonverbal Behavior* **34**:15–26, 2010. https://doi.org/10.1007/s10919-009-0077-y

[7] S. P. Hoogendoorn, P. H. L. Bovy. Pedestrian route-choice and activity scheduling theory and models. *Transportation Research Part B: Methodological* **38**(2):169–190, 2004. https://doi.org/10.1016/S0191-2615(03)00007-9

[8] G. Johansson. Visual perception of biological motion and a model for its analysis. *Perception & psychophysics* **14**(2):201–211, 1973. https://doi.org/10.3758/BF03212378

[9] C. de'Sperati, P. Viviani. The relationship between curvature and velocity in two-dimensional smooth pursuit eye movements. *Journal of Neuroscience* **17**(10):3932–3945, 1997. https://doi.org/10.1523/JNEUROSCI.17-10-03932.1997

[10] D. Huh, T. J. Sejnowski. Spectrum of power laws for curved hand movements. *Proceedings of the National Academy of Sciences* **112**(29):E3950–E3958, 2015. https://doi.org/10.1073/pnas.1510208112

[11] C. Feliciani, K. Shimura, K. Nishinari. *Introduction to crowd management: Managing crowds in the digital era: Theory and Practice*. Springer Nature, 2022. https://doi.org/10.1007/978-3-030-90012-0

[12] D. R. Parisi, P. A. Negri, L. Bruno. Experimental characterization of collision avoidance in pedestrian dynamics. *Physical Review E* **94**(2):022318, 2016. https://doi.org/10.1103/PhysRevE.94.022318

[13] J. Chen, Q. Luo, Q. Wang, et al. Experimental study on individual and crowd movement features around obstacles with different shape and size. *Physica A: Statistical Mechanics and its Applications* **645**:129797, 2024. https://doi.org/10.1016/j.physa.2024.129797

[14] A. Corbetta, J. A. Meeusen, C.-m. Lee, et al. Physics-based modeling and data representation of pairwise interactions among pedestrians. *Physical review E* **98**(6):062310, 2018. https://doi.org/10.1103/PhysRevE.98.062310

[15] A. Corbetta, C.-m. Lee, R. Benzi, et al. Fluctuations around mean walking behaviors in diluted pedestrian flows. *Physical Review E* **95**(3):032316, 2017. https://doi.org/10.1103/PhysRevE.95.032316

[16] H. Hicheur, S. Vieilledent, M. J. E. Richardson, et al. Velocity and curvature in human locomotion along complex curved paths: a comparison with hand movements. *Experimental brain research* **162**(2):145–154, 2005. https://doi.org/10.1007/s00221-004-2122-8

[17] V. Ziemer, A. Seyfried, A. Schadschneider. Congestion dynamics in pedestrian single-file motion. In *Traffic and Granular Flow'15*, pp. 89–96. Springer, 2016. https://doi.org/10.1007/978-3-319-33482-0_12

[18] T. Kanda, D. Brščić. Data set: Pedestrian tracking with group annotations, 2015. [2025-08-30]. https://dil.atr.jp/ISL/sets/groups/

[19] F. Zanlungo, T. Ikeda, T. Kanda. Potential for the dynamics of pedestrians in a socially interacting group. *Physical Review E* **89**(1):012811, 2014. https://doi.org/10.1103/PhysRevE.89.012811

[20] L. Hao, B. Huang, B. Jia, G. Mao. On the fine-grained crowd analysis via passive WiFi sensing. *IEEE Transactions on Mobile Computing* **23**(6):6697–6711, 2023. https://doi.org/10.1109/TMC.2023.3324334

[21] D. Gonon, A. Billard. Inverse reinforcement learning of pedestrian–robot coordination. *IEEE Robotics and Automation Letters* **8**(8):4815–4822, 2023. https://doi.org/10.1109/LRA.2023.3289770

[22] D. F. Glas, F. Ferreri, T. Miyashita, et al. Automatic calibration of laser range finder positions for pedestrian tracking based on social group detections. *Advanced Robotics* **28**(9):573–588, 2014. https://doi.org/10.1080/01691864.2013.879272

[23] JR West Japan. JR West in data, 2023. [2025-05-20]. https://www.westjr.co.jp/company/info/issue/data/

[24] Osaka Metro. Number of passengers by line and station, 2024. [2025-05-20]. https://www.osakametro.co.jp/company/statistics/research/100331_research.php

[25] Hankyu railways. Number of passengers by station, 2024. [2025-05-20]. https://www.hankyu.co.jp/station/passenger/index.html

[26] Hanshin railways. Number of passengers by station, 2023. [2025-05-20]. https://www.hanshin.co.jp/company/pdf/handbook_all.pdf

[27] D. F. Glas, T. Miyashita, H. Ishiguro, N. Hagita. Laser-based tracking of human position and orientation using parametric shape modeling. *Advanced robotics* **23**(4):405–428, 2009. https://doi.org/10.1163/156855309X408754

[28] G. G. M. van der Vleuten, F. Toschi, W. Schilders, A. Corbetta. Stochastic fluctuations of diluted pedestrian dynamics along curved paths. *Physical Review E* **109**(1):014605, 2024. https://doi.org/10.1103/PhysRevE.109.014605

[29] A. Savitzky, M. J. E. Golay. Smoothing and differentiation of data by simplified least squares procedures. *Analytical chemistry* **36**(8):1627–1639, 1964. https://doi.org/10.1021/ac60214a047

[30] B. A. Dubrovin, A. T. Fomenko, S. P. Novikov. *Modern Geometry – Methods and Applications*, vol. 93. Springer Science & Business Media, 1984.

[31] F. Zanlungo, T. Ikeda, T. Kanda. A microscopic "social norm" model to obtain realistic macroscopic velocity and density pedestrian distributions. *PloS one* **7**(12):e50720, 2012. https://doi.org/10.1371/journal.pone.0050720

[32] Z. Yücel, F. Zanlungo, M. Shiomi. Modeling the impact of interaction on pedestrian group motion. *Advanced Robotics* **32**(3):137–147, 2018. https://doi.org/10.1080/01691864.2017.1421481

[33] Z. Yücel, F. Zanlungo, C. Feliciani, et al. Identification of social relation within pedestrian dyads. *PloS one* **14**(10):e0223656, 2019. https://doi.org/10.1371/journal.pone.0223656

[34] P. Zhao, L. Sun, L. Cui, et al. The walking behaviours of pedestrian social group in the corridor of subway station. In *Proceedings of the 2016 Pedestrian and evacuation dynamics conference*, pp. 34–40. 2016. https://doi.org/10.17815/CD.2016.11